Modeling High-Pressure Microplasmas: Comparison of Fluid Modeling and Particle-in-Cell Monte Carlo Collision Modeling

Yong Jun Hong, Seung Min Lee, Gyoo Cheon Kim, Jae Koo Lee*

The results of simulations using a fluid model and a PIC-MCC model are compared, and the PIC-MCC is used to explore the kinetics of energetic ions and electrons in microplasmas. The kinetics are studied under helium discharges at 760 Torr and Ne/Xe DBD discharges at 300 Torr with various driving currents and geometries. While EEPFs of microplasmas at high pressure show strong nonequilibrium behavior near the sheath region, EEDFs on the powered and grounded electrodes have qualitatively different features depending on input power. The effective temperature and energy flux of charged particles can be obtained from the slopes in EEPFs and IEPFs. The effects of input power, discharge length, and mixture gas concentration on the IEDFs on each electrode are discussed.

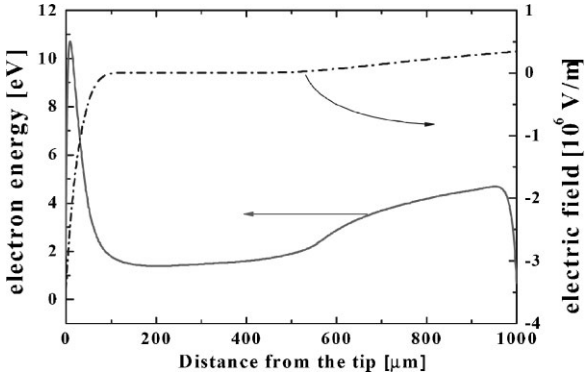

Introduction

Microdischarges generally typically range from a few micrometers to a few millimeters. Paschen's breakdown law[1] indicates that plasmas in small systems are easy to generate at high pressure. When characteristic lengths are hundreds of micrometers, the discharges can naturally operate at atmospheric pressure and contain highly reactive components such as charged particles and excited species, radicals, and photons. Microplasmas can be sustained by low-power sources and can be adapted for portable devices, because they are small and do not require vacuum pumps.

The plasma needle jet is one type of nonthermal plasma that operates at atmospheric pressure; it has a single electrode configuration and is operated in helium.[2–5] Plasma needle jets emit a plasma that allows treatment of irregular surfaces and has a small penetration depth. Therefore, they have been widely used for biomedical applications. Plasma needle jets are capable of bacterial decontamination and localized cell removal without killing tissues.[4] One of the present authors showed in unpublished work that dental calculus was removed more easily after brief plasma treatment than without the plasma treatment. We hypothesized that charged particles, radicals, and emitted UV light or electric field interact with the cell membranes and cell adhesion molecules (CAMs), and therefore cause cell detachment. Kieft et al.[5]

Y. J. Hong, S. M. Lee, G. C. Kim, J. K. Lee
Department of Electronic and Electrical Engineering, Pohang University of Science and Technology, Pohang 790-784, Republic of Korea
Fax: +82 54 279 2903; E-mail: jkl@postech.ac.kr
Y. J. Hong
Current address: Department of Physics, Pohang University of Science and Technology, Pohang 790-784, Republic of Korea
G. C. Kim
Current address: Department of Oral Anatomy, College of Dentistry, Pusan National University, Busan 602-739, Republic of Korea

© 2008 WILEY-VCH Verlag GmbH & Co. KGaA, Weinheim
DOI: 10.1002/ppap.200800024

noted that the mechanism of cell detachment is expected to be a result of plasma chemistry, and that the plasma effect on cell adhesion was closely connected with species emitted from the plasma, and not to other plasma-related factors such as UV light and electric field. To distinguish between these two explanations, our interest was to determine the characteristics of the plasma needle jet. To do this, we compared the plasma characteristics as simulated using two simple models.

Many research papers have reported the kinetics of low-pressure discharges using either experimental methods or computational simulations.[6,7] However, appropriate collisional probe theories at high pressure are insufficient and the spatial resolution of optical measurement cannot always resolve the characteristics of microplasmas. Computer simulations provide an alternative method for analyzing microplasmas at high pressure and for contributing to the understanding of the underlying physics by providing spatially resolved kinetic information. Most simulations have used fluid models for the diagnostics of low-temperature plasmas because of their advantage in computational speed.[8–13] Fluid models can also consider a large number of species; this allows the study of complicated chemistries with numerous reactions. An alternative approach is to use particle-in-cell Monte Carlo collision (PIC-MCC) simulations. Although this type of simulation is more difficult, it models statistical processes in more detail than do fluid simulations.

In low-pressure plasmas, each species is typically far from thermal equilibrium, and velocity distributions deviate from Maxwellian.[6,7,14] Because fluid simulations are based on the value of the local electric field or the local energy dissipation, they cannot capture the nonlocal effects that are often encountered in low-pressure plasmas. PIC-MCC simulations have produced results comparable to experimental data in low-pressure plasmas. Fluid models are suited for relatively high-pressure discharges such as the plasma display panels because nonlocal effects are not usually dominant.[8,9,15,16] When using fluid and PIC-MCC models at high pressure, even atmospheric pressure, it is necessary to quantify the differences and similarities of the results obtained by the two modeling methods.

We first verify our fluid simulations modeled with analogous conditions of PIC-MCC simulations by comparing output to published results.[12,13] Because the present version of our PIC-MCC simulation tool can deal only with charged particles, we need to compare the simulation results using our simplified fluid model to results produced by other fluid model simulations of more complicated reactions. We used the PIC-MCC model under the same conditions and compared the results to those of the fluid simulations. We also used the PIC-MCC model to simulate electron and ion kinetics in high-pressure microplasmas.

This article is organized as follows. In the next section, simulation models and several types of discharge conditions are presented. Comparison of results obtained from fluid model and PIC-MCC model are described in the following section. Electron and ion kinetics obtained by computational calculation in various types of microplasmas are compared and discussed in the subsequent parts. Finally, conclusions and future trends are discussed.

Simulation Models and Discharge Conditions

Fluid Models

Fluid models solve continuity equations, and flux and energy equations for each species in the plasma.[12,17] Poisson's equation is coupled with these fluid equations to obtain self-consistent electric fields. To simplify computation, the drift-diffusion approximation is typically used instead of the flux balance equation, because the momentum transfer collisional frequency is much larger than the RF driving frequency in atmospheric pressure plasmas.[17] The continuity equation gives plasma density information for each time step. The plasma density is determined by the variation of the flux and the plasma source, which affects loss and reproduction of each species.

To calculate the source term in the continuity equation and the transport coefficients in the flux equation, such as the mobility and the diffusion constants, the average collisional frequencies (e.g., ionization and momentum transfer collisional frequencies) must be determined by averaging over the velocity (energy) distribution; a suitable velocity distribution must be assumed. In our fluid model, we assumed a Maxwellian distribution of particle velocity or energy distribution, then solved the energy equation to determine the various frequencies and transport coefficients as a function of the temperature (mean particle energy).[12] The average electron energy is determined by the energy equation using the particle flux; the electric field calculated in Poisson's equation; and collisional losses, including elastic energy losses due to collisions with background gases and inelastic energy losses due to excitation and ionization. Consequently, the plasma density, potential, electron energy and the other characteristics of plasmas can be analyzed as a function of position due to the correlation of each equation.

PIC-MCC Model

Because the details of the PIC-MCC method have been described in several papers,[18,19] only the most important features are presented here. PIC simulations take advantage of the collective behavior of charged particles in

Plasma Process. Polym. **2008**, *5*, 583–592
© 2008 WILEY-VCH Verlag GmbH & Co. KGaA, Weinheim
DOI: 10.1002/ppap.200800024

plasmas to model the kinetics of various species by simulating a reduced number of particles. Collisions are incorporated in the simulation by applying an MCC scheme, which determines statistically the particles undergoing collisions and their scattered velocities. The interaction between the particles and the surface of each electrode is also modeled at the boundaries. In this paper, the kinetic information was obtained using one-dimensional (1d3v) PIC-MCC simulation.[6,7,17,20–22] We assumed that a neutral gas was distributed uniformly over the discharge space with a temperature of 0.026 eV. To reduce the computational cost of PIC-MCC simulation of particle kinetics, we considered electrons and single-positive ions as charged particles. For the electron collisions with neutral gases, we considered the elastic, excitation, and ionization collisions. Momentum transfer and charge exchange collisions were used to model ion collisions with neutral gases.

Simulation Conditions Used in Both Models

To simulate the needle discharges, we used one-dimensional fluid and PIC-MCC models in a cylindrical coordinate system because the large aspect ratio of the needle tip to the grounded plate should be considered. Both simulation models used the same discharge condition: an inner electrode with a radius of 0.03 mm was powered by RF (13.56 MHz) current sources of 0.35 $A \cdot cm^{-2}$ (0.02 mA) and 0.88 $A \cdot cm^{-2}$ (0.05 mA); a grounded outer electrode with a radius of 1.03 or 0.53 mm, and a cylinder of 0.03 mm length. The gap distances between the electrodes were 1 or 0.5 mm. The background gas was neutral helium at a pressure of 760 Torr. To simplify the PIC-MCC simulation, we considered only helium ions and electrons. To facilitate comparison of the results of the two models, the fluid model also included only these charged particles.

Simulation Conditions Used Only in PIC-MCC

Other microplasma devices were simulated only by PIC-MCC simulation. DC and RF (13.56 MHz) driven capacitive coupled helium discharges between parallel palates were obtained by applying a 1 $A \cdot cm^{-2}$ current source at atmospheric pressure. System size was 200 μm.[20,21] The dielectric barrier discharge (DBD) was also sustained in an Ne/Xe mixture at 300 Torr (39.9 kPa). The Xe concentration was 5, 10, or 20% and the discharge configuration corresponds to a parallel-plate reactor with electrodes covered with 30 μm dielectrics ($\varepsilon_r = 10$).[23] The distance between the two parallel electrodes was 200 μm, and the discharge was driven by 200 V bipolar square pulses of 3 μs duration with rising and falling times of 50 ns. Constant ion-induced secondary electron emission coefficients $\gamma He^+ = 0.1$ were used. A coefficient of secondary-electron emission that accounts for the energy and angle of the incident ions was used only for the Ne/Xe DBD discharges.[8] The PIC-MCC model does not consider secondary electron emission processes of discharges which occur at high pressure, such as contributions from ions, metastables, hot neutrals, and photons; these factors be included in future refinements of this model.

Results and Discussion

Comparison of Fluid and PIC-MCC Model

Fluid Model

Simulated mean electron density peaked near the tip, showing a broad second peak near the outer electrode (Figure 1). The electrical field was very strong near the tip ($-3.36 \times 10^6 \cdot V \cdot m^{-1}$) but was relatively constant at several thousands of volts per meter at more than about 100 mm from the tip. These results are similar to those of Sakiyama and Graves who simulated electrical fields using a one-dimensional fluid model which considered several species.[12,13] The discharge conditions in ref.[12] were different from ours: 1 000 mW power source in spherical geometry. Nonetheless, the model produced results that are qualitatively similar to ours, although some differences can be noted. Sakiyama and Graves observed a second peak of mean electron energy and electric field profile near the outer electrode, and suggested that it was related to a density profile of metastable species there. The maximum density values of charged particles modeled by us and Sakiyama's are within the same order of magnitude. The similarity between the results of our simplified fluid model and the more detailed Sakiyama model verifies that our model provides realistic results and can be used to help

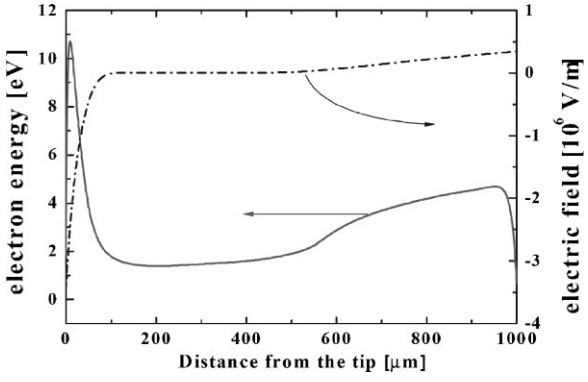

Figure 1. Time-averaged mean electron energy (solid line) and electric field (dashed line) at 0.05 mA; 1 mm gap.

© 2008 WILEY-VCH Verlag GmbH & Co. KGaA, Weinheim

understand the characteristics of high-pressure plasma discharge.

Particle-in-Cell Model

When using PIC-MCC models, time consumption is a significant problem when simulating millimeter size discharge at high pressures, including atmospheric pressure. The large time consumption complicates attempts to account for various chemical species and reactions; therefore, only charged particles are considered in our PIC-MCC model. Because we have verified that the results obtained by our simple fluid model agree with those of a more detailed fluid model that considers more ions and excited species,[12] we use our simple fluid model as a standard against which to evaluate the results obtained by our PIC-MCC model. If the results of the PIC-MCC model are similar to those of the simple fluid model, we conclude that they are also similar to those of the complex fluid model[12] and therefore that PIC-MCC gives meaningful output which can be used to understand the high-pressure plasma physics of microplasmas.

Due to variations of input current value and system length in microplasma devices, we used both the PIC-MCC and fluid models to simulate all four combinations of low (0.02 mA) or high (0.05 mA) current and large (1 mm) or small (0.5 mm) gap size. All the simulations assume asymmetric electrodes at atmospheric pressure, and output time-averaged profiles of each species density, of potential and of electric field (Figure 2–5).

Where the current is low and the gap is large, the potential and electric field profiles in both simulation models are similar (Figure 2), although the quantitative values differ slightly. The peak potential at the sheath edge is 41 V in the fluid model and 33 V in the PIC-MCC model (Figure 2b). The potential value on the inner electrode is −56 V in the fluid model and −136 V in the PCI-MCC model (Figure 2b). The electric field reaches a minimum on the inner electrode and a relatively low positive electric field profile appears on the outer electrode (Figure 2c): on the inner electrode, it is $-2.81 \times 10^6\ \mathrm{V \cdot m^{-1}}$ in the fluid model and $-4.03 \times 10^6\ \mathrm{V \cdot m^{-1}}$ in the PIC-MCC model; on the outer electrode, it is $1.43 \times 10^5\ \mathrm{V \cdot m^{-1}}$ in the fluid model and $8.71 \times 10^4\ \mathrm{V \cdot m^{-1}}$ in the PIC-MCC model. Because the high electric field causes electron and ion impact ionization reactions near the inner electrode, the density profiles of both simulation models show a peak there (Figure 2a). The ion densities are quite similar, but the electron density predicted by fluid model is about twice as great as predicted by PIC-MCC simulation.

When current is high and the gap is large, the electric field profiles are very similar, but the potential profiles obtained by the two simulations are different (Figure 3). On the inner electrode, the maximum value of high electric field is $-3.36 \times 10^6\ \mathrm{V \cdot m^{-1}}$ in the fluid model and

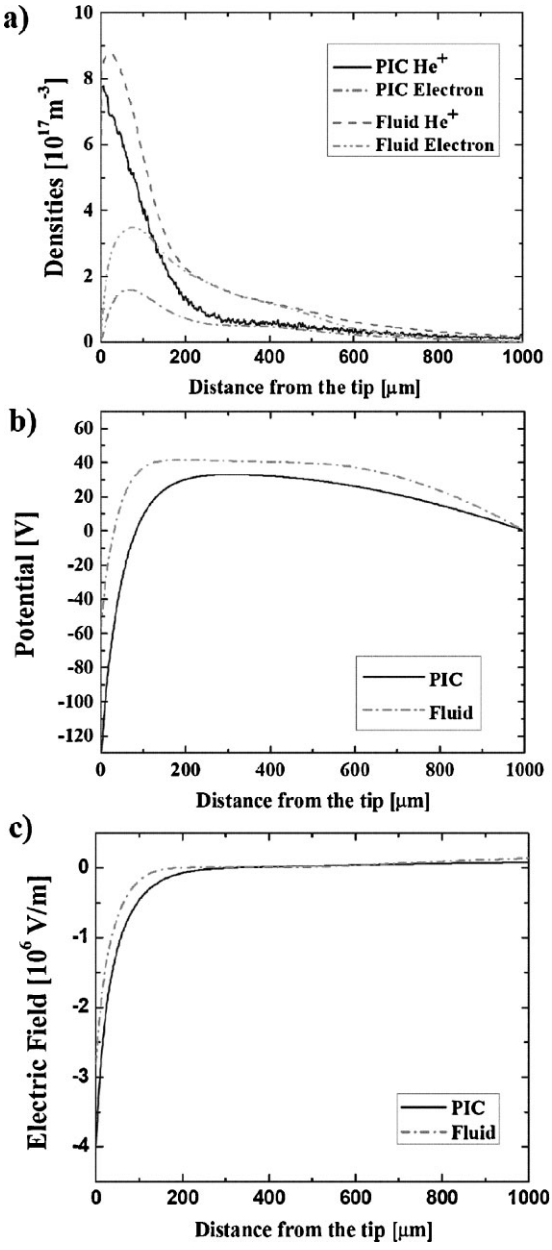

Figure 2. Comparison of PIC and fluid simulation results at 0.02 mA (low current), 1 mm (long distance) gap: (a) discharge density profiles of each species, (b) potential profiles, and (c) electric field profiles as a function of distance from the tip to the grounded electrode.

$-5.36 \times 10^6\ \mathrm{V \cdot m^{-1}}$ in the PIC-MCC model (Figure 3c). The electric fields on the outer electrode are near $3 \times 10^5\ \mathrm{V \cdot m^{-1}}$ in both simulations. However, the potential profiles in Figure 3 are different from those in Figure 2. The minima on the inner electrode are commonly positive in Figure 3: 4.61 V in the fluid simulation and 91.8 V in the PIC simulation. The positive minima in Figure 3 are distinct from the negative minima in Figure 2. The density profiles in Figure 2 and 3 are also different. Unlike the case of the

© 2008 WILEY-VCH Verlag GmbH & Co. KGaA, Weinheim
DOI: 10.1002/ppap.200800024

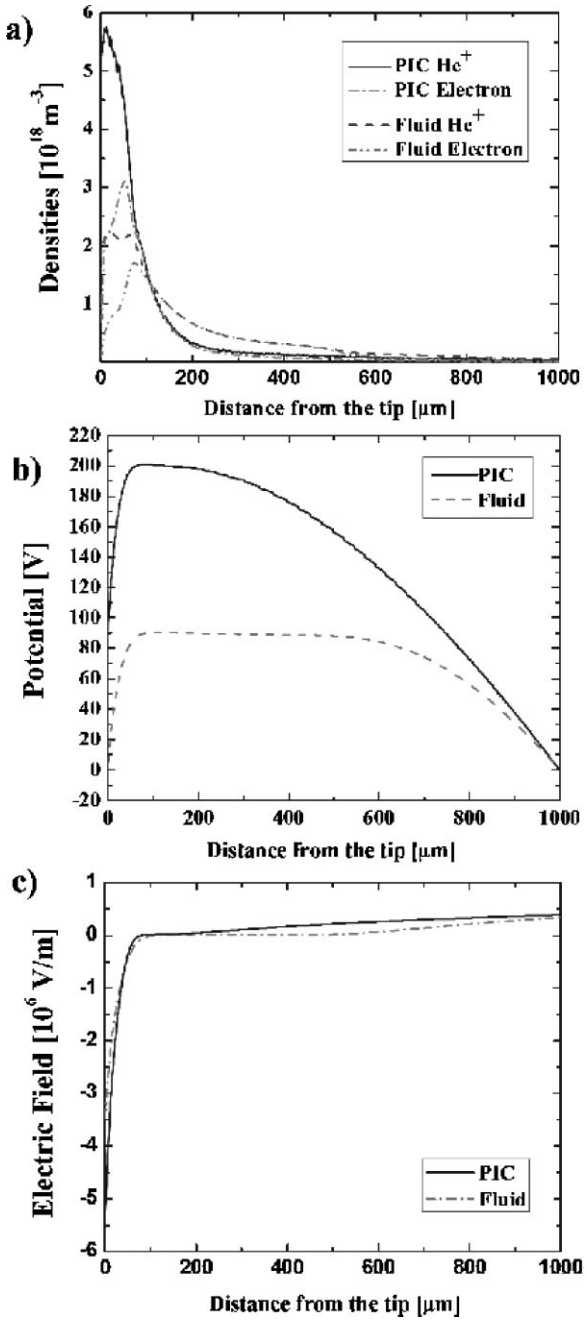

Figure 3. Comparison of PIC and fluid simulation results at 0.05 mA (high current), 1 mm (long distance) gap: (a) discharge density profiles of each species, (b) potential profiles, and (c) electric field profiles as a function of distance from the tip to the grounded electrode.

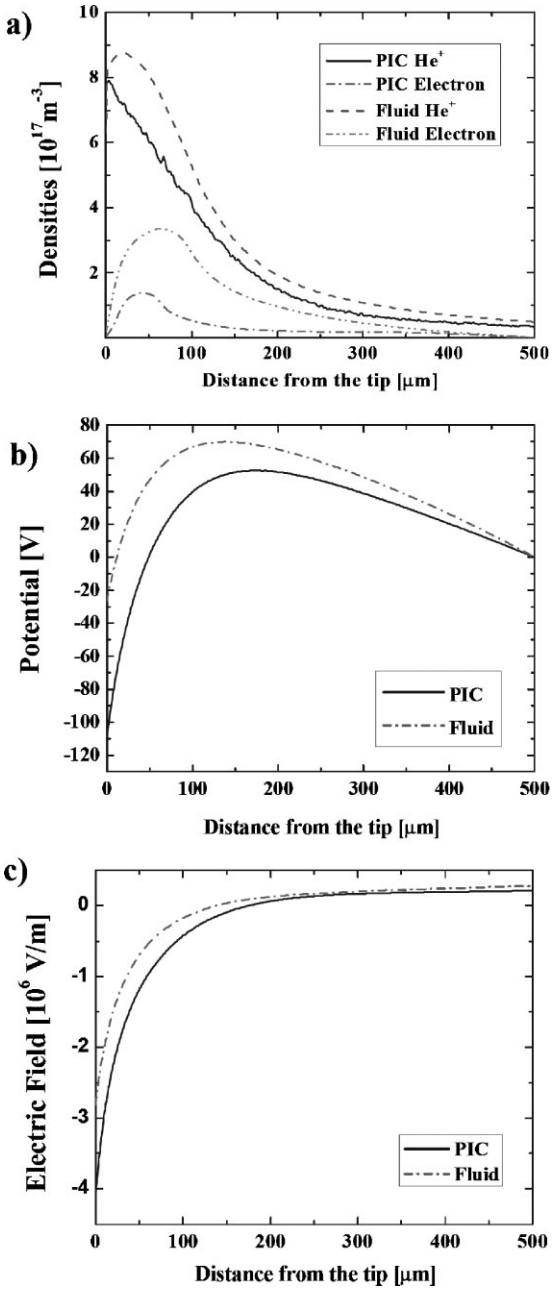

Figure 4. Comparison of PIC and Fluid simulation results at 0.02 mA (low current), 0.5 mm (short distance) gap: (a) discharge density profiles of each species, (b) potential profiles, and (c) electric field profiles as a function of distance from the tip to the grounded electrode.

low current mode (Figure 2a), the density profile predicted by the PIC-MCC simulation is higher than that by the fluid simulation.

These features are also shown in the results obtained in simulations of small gap length (Figure 4 and 5). When the input current is low, the density and potential profiles predicted by the fluid simulation are a little higher than those by the PIC-MCC simulation, whereas when the current is high, the density and potential profiles obtained by fluid simulation are much lower than those obtained by the PIC-MCC simulation. We attribute this distinction to the assumption of a Maxwellian distribution in the fluid model. When the input current is low, the relatively linear falling slopes of the energy distributions on the inner

© 2008 WILEY-VCH Verlag GmbH & Co. KGaA, Weinheim

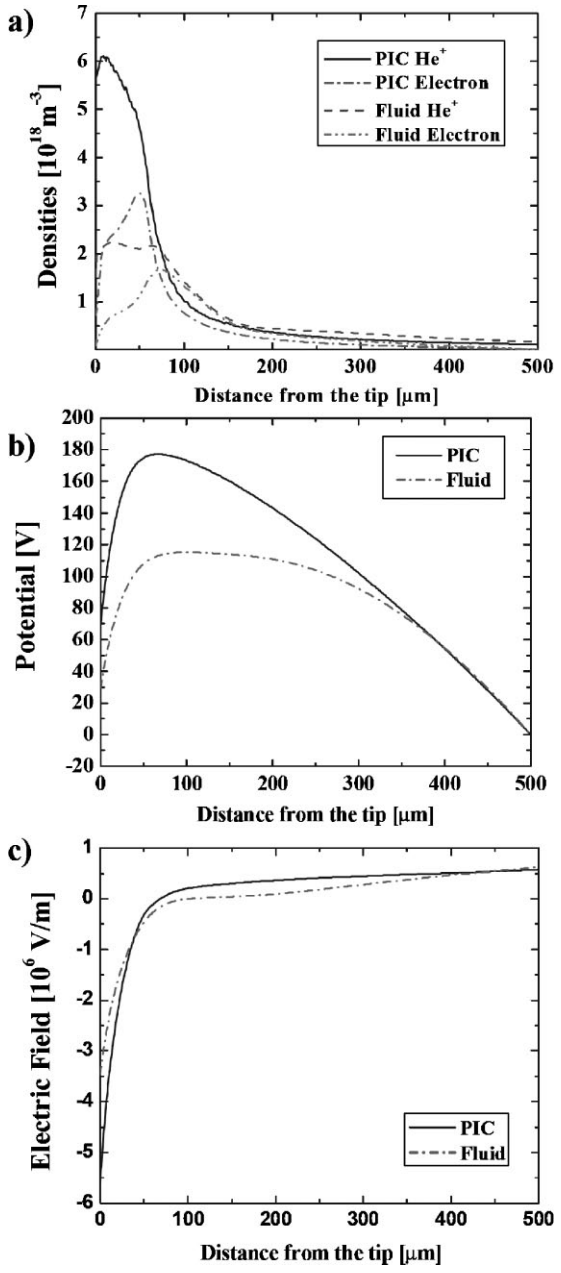

Figure 5. Comparison of PIC and fluid simulation results at 0.05 mA (high current), 0.5 mm (short distance) gap: (a) discharge density profiles of each species, (b) potential profiles, and (c) electric field profiles as a function of distance from the tip to the grounded electrode.

electrode occur regardless of gap size (Figure 2b, 4b, and 6). The results obtained from the PIC-MCC and fluid simulation models are qualitatively similar. When the current is high, the energy distributions have two different slopes (Figure 6), which do not correspond to Maxwellian distributions. Many more electrons exist in the low energy part of electron energy distribution functions (EEDFs) on the powered electrode, and this causes a big difference in the density profiles simulated by the PIC-MCC and fluid models.

Time-averaged electron and ion power absorption density profiles were obtained by both the PIC-MCC and fluid simulations, which showed similarity except for the middle of the discharges at the high current (Figure 7). While most of the ion power is dissipated near the inner electrode, the electron power absorption spreads over the discharge region. Although the second broad peak of the PIC simulation results is somewhat ambiguous (Figure 7b and d), the fluid simulation at the high current, unlike those at the low current (Figure 7a and c), shows the second broad peak of ion power absorption near the outer electrode.

Kinetic Information from the PIC-MCC Model

Plasma Needle Jet Simulation

The PIC-MCC simulation yields the kinetic information such as the energy distribution (Figure 6). Because fluid models are based on a certain assumption of the particle velocity of energy distribution, which appears invalid, the particle kinetics must be understood in order to reveal the underlying physics governing these discharges. Despite differences in system length, the electron and ion energy distribution on the inner electrode clearly differ in the low and high current modes. Due to the high collisionality at the atmospheric pressure, the charged particles that strike the electrode have a low enough energy to minimize erosion of the electrode and result in a long lifetime of a device. While the maximum energy of electrons striking the inner electrode is about 20 eV in any case, the ion maximum energy is about 5 eV if the current is 0.02 mA and 10 eV if it is 0.05 mA. The energy distributions of charged particles striking the outer electrode show different features for each discharge condition (Figure 6b and d). As the distance from the powered electrode to the grounded electrode decreases or the input current source increases, more energetic ions can reach the grounded (outer) electrode.

The simulated energy distributions can be used to calculate effective temperatures and energy flux for the charged particles striking each electrode.[1] The effective electron temperatures on the outer electrode are higher than those on the inner electrode, while the effective ion temperatures on the outer electrode are much lower than those on the inner electrode (Table 1). The effective ion temperatures on the outer electrode are in the range of 0.04–0.06 eV. When the ion temperatures near the outer electrode are obtained from linear fits to the simulated ion energy probability functions (IEPFs), they are near room temperature (≈0.026 eV).

© 2008 WILEY-VCH Verlag GmbH & Co. KGaA, Weinheim
DOI: 10.1002/ppap.200800024

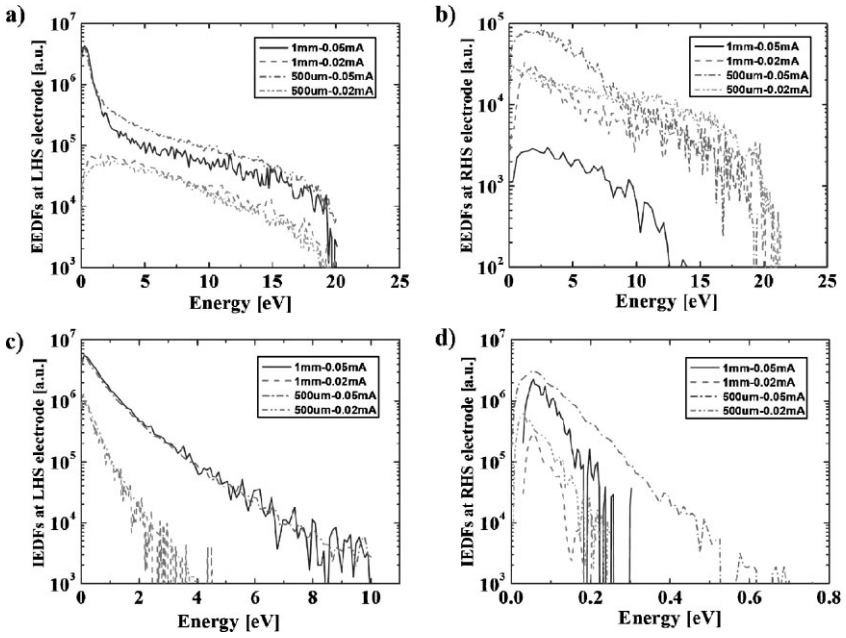

Figure 6. Comparison of energy distribution of PIC simulation results for each discharge condition: (a) electron energy distribution on the powered electrode (inner radius), (b) electron energy distribution on the grounded electrode (outer radius), (c) ion energy distribution on the powered electrode (inner radius), and (d) ion energy distribution on the grounded electrode (outer radius).

The energy flux is one important piece of information required to understand the interaction of charged particles with surface of material upon the outer electrode in potential biomedical fields, material processing, and analytical applications, while the flux toward the opposite electrode affects the lifetime of a device. At a constant current, the calculated energy flux on both electrodes increases with decrease in system length (Table 2). With current increasing from 0.02 to 0.05 mA, most ion number and energy fluxes increase but the electron fluxes do not, because the lower potentials at both electrodes than in the bulk favor low electron number and energy fluxes.

Simulations of Various High-Pressure Plasmas

Electron kinetics is very important in plasma physics. Simulations presented in this section reveal that the electron energy probability functions (EEPFs) in

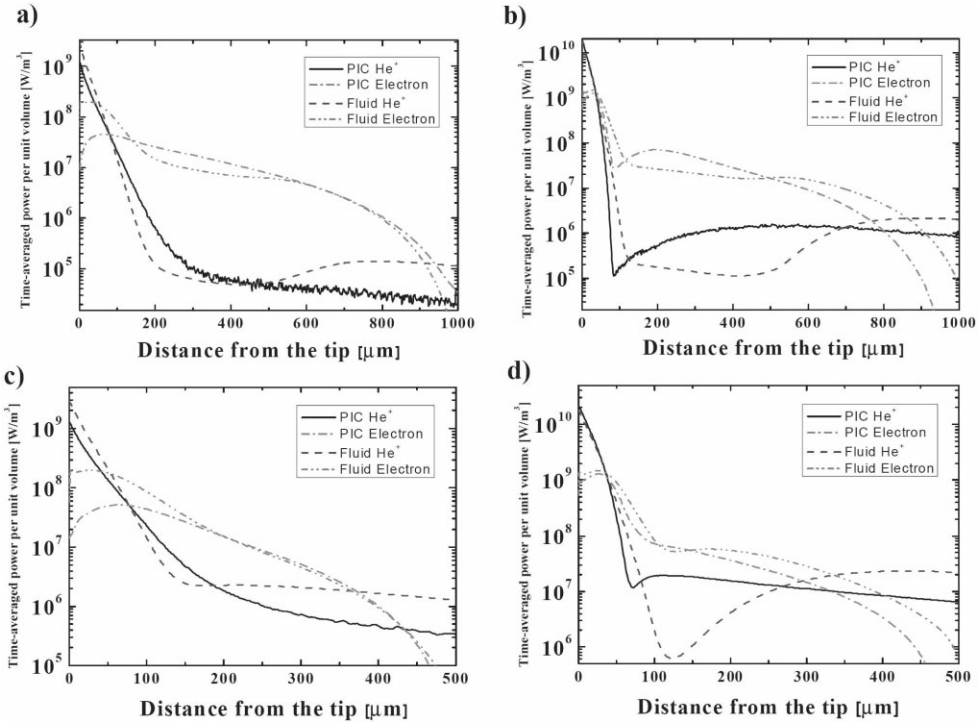

Figure 7. Comparison of time-averaged power density profiles of PIC and fluid simulation results (a) at 0.02 mA (low current) and 1 mm (long distance) gap, (b) at 0.05 mA (high current) and 1 mm (long distance) gap, (c) at 0.02 mA (low current) and 0.5 mm (short distance) gap, and (d) at 0.05 mA (high current) and 0.5 mm (short distance) gap.

© 2008 WILEY-VCH Verlag GmbH & Co. KGaA, Weinheim

Table 1. Effective temperatures of helium ions and electrons calculated using the energy distribution function obtained from the PIC-MCC simulation. Inner electrode is powered and outer electrode is grounded.

Gap size	Current	Effective temperature			
mm	mA	eV			
		Inner Electrode		Outer Electrode	
		He^+	e^-	He^+	e^-
1.0	0.02	0.282	3.80	0.0484	3.97
1.0	0.05	0.602	1.42	0.0560	3.05
0.5	0.02	0.287	3.79	0.0414	4.66
0.5	0.05	0.593	1.94	0.0637	2.82

various microplasmas have very similar shapes despite the differences in discharge conditions.

It is normally accepted that low-pressure discharges depend on nonlocal kinetics, whereas high-pressure microdischarges depend on the local kinetics simply because the mean free path of electrons is very short in the range of several hundreds torr. However, microplasmas at atmospheric pressure can have spatially nonlocal characteristics in which high energy electrons survive in the center of the discharges when the sheath size is comparable to the system gap size.[20] In high-pressure microplasmas, even at atmospheric pressure, the electrons are not in local equilibrium with the electric field. In our simulations, the EEPFs in the bulk and at the sheath edge of all the microplasmas reveal strong nonequilibrium characteristics with multiple temperatures.[20,21,24] Numerous low-energy electrons are confined in the bulk because of typical ambipolar potential, whereas mid-energy electrons have higher temperature than the low-energy electrons and energy large enough to escape the bulk region. High-energy electrons are generated by acceleration in the sheath of secondary electrons emitted from electrodes. These electrons penetrate only a short distance into the bulk ($L \approx 1$ mm or 200 μm $\gg \lambda_\varepsilon \approx 1$ μm) in DC and RF atmospheric discharges with gap over 200 μm.[20,21,24]

When the gap size was 1 mm, the EEPFs in the plasma needle discharges resembled those in DC and RF atmospheric microplasmas. While the EEPFs at the sheath edge of microdischarges show the three-temperature shapes, those in the center of the discharges do not have the high energy tail (Figure 8 and 9).[20,21] The characteristics of gases cause each electron energy group in the EEPF at the sheath edge. The first electron group has very low energy, and is commonly affected by ambipolar potential, and sometimes belongs to nonlocal regime ($\lambda_\varepsilon > L$) when the gap size is comparatively short. The second energy groups (Figure 8 and 9) are distinctively located in each EEPF, because the knee between low and high-energy electrons is determined by the excitation threshold energy of each gas (Xe ≈ 8 eV, Ar ≈ 12 eV, Ne ≈ 16 eV, and He ≈ 20 eV).

While electron kinetics is important in determining the volumetric characteristic of discharges, ion kinetics provides information on the plasma-surface interaction of materials. The ion energy distribution function (IEDF) on the electrode is important in various plasma systems. The IEDF obtained by the PIC-MCC simulation has some different characteristics as well as common features. High energetic ions disappear as pressure increases (Figure 6 and 10).[21] This occurs because increase in the pressure raises the neutral gas density and then enhances the collisionality. In the case of atmospheric helium microplasmas sustained by current density of $\approx 1\ A \cdot cm^{-2}$, IEDFs are very similar to those shown in Figure 6c and Choi et al.[21] RF microdischarges can be regarded as a succession of DC discharges at various powers because the RF discharges are time modulated.[20,24]

Table 2. Energy flux of helium ions and electrons calculated using the energy distribution function obtained from the PIC-MCC simulation. Inner electrode is powered and outer electrode is grounded.

Gap size	Current	Energy Flux			
mm	mA	$eV \cdot m^{-2} \cdot s^{-1}$			
		Inner Electrode		Outer Electrode	
		He^+	e^-	He^+	e^-
1.0	0.02	5.12×10^{20}	1.27×10^{21}	6.90×10^{16}	6.80×10^{19}
1.0	0.05	1.11×10^{22}	2.37×10^{22}	8.00×10^{17}	6.32×10^{18}
0.5	0.02	6.49×10^{20}	5.79×10^{21}	3.31×10^{17}	2.31×10^{20}
0.5	0.05	1.01×10^{22}	3.69×10^{22}	4.60×10^{18}	2.79×10^{20}

© 2008 WILEY-VCH Verlag GmbH & Co. KGaA, Weinheim
DOI: 10.1002/ppap.200800024

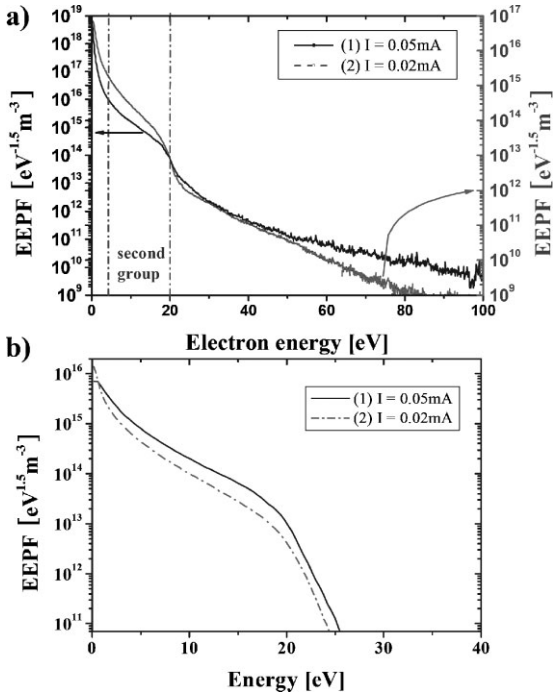

Figure 8. EEPFs (a) at the sheath edge and (b) in the center of He plasma needle discharges of 1 mm gap at atmospheric pressure (760 Torr).

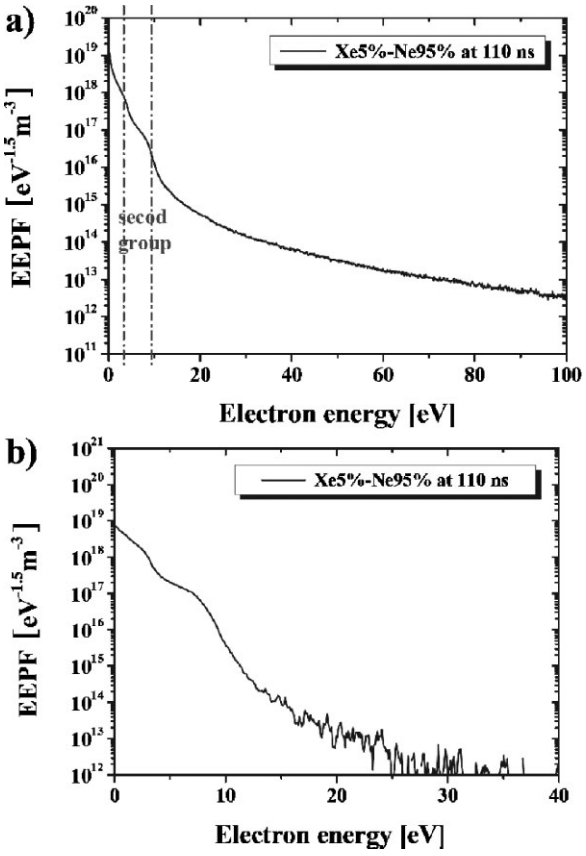

Figure 9. EEPF (a) at the sheath edge and (b) in the center of DBD discharge of mixture gas of Xe (5%) and Ne (95%) at 300 Torr.

IEDFs in DBD discharges are affected by varying Xe in the content (Figure 10). Although the concentration of neutral Ne is higher than that of neutral Xe, a large number of Xe ions are produced and more Xe ions than Ne ions arrive in the cathode region because the ionization cross-section of Xe is greater than that of Ne. Ne ions cannot reach high energy because of the resonant charge exchange between neutral Ne and ions in the cathode sheath region (Figure 10a). As the concentration of Xe increases, the high energy tail of the Xe ion distribution decreases, while that of Ne ion increases. High-energy ions occur in the cathode fall of microplasmas at a pressure less than atmospheric pressure. Through these simulation results, we note that IEDFs on the cathode depend on the pressure despite the difference in geometrical configurations, when the input power is same and the effect of gas species such as ion-neutral cross-section is not important.

Conclusion

This paper has presented a comparison of simulated electron and ion kinetics in the DC, pulsed DC, and RF microplasma sources at high pressures. EEPFs of various microplasmas at high pressure including atmospheric pressure show a three-temperature shape. Compared to low-pressure discharge, which has a high energy tail that is not in equilibrium with the local electric field, it should be considered that microplasmas at higher pressures also have nonequilibrium characteristics, even at atmospheric pressure.

Although different types of power were applied, ion kinetics on the electrode of each discharge also show the similarity that ion energy distributions of microplasmas are Maxwellian with one ion temperature. As the pressure of microplasmas increases, the number of energetic ions and the ion temperature both decrease. Simulated maximum ion energy of atmospheric pressure microplasmas is almost 10 eV and the ion energy on the grounded electrode in the plasma needle discharge is less than 1 eV.

Microplasmas have high reactivity, low-gas temperature, and nonequilibrium characteristics. Microplasma devices can also be portable due to elimination of the vacuum pump. For these reasons, microplasmas have potential applications in various practical devices. Particle kinetics must be understood in order to resolve the underlying physics governing these discharges. Along with good experimental methods, computational research is essential for understanding the physics behind plasmas. After

© 2008 WILEY-VCH Verlag GmbH & Co. KGaA, Weinheim

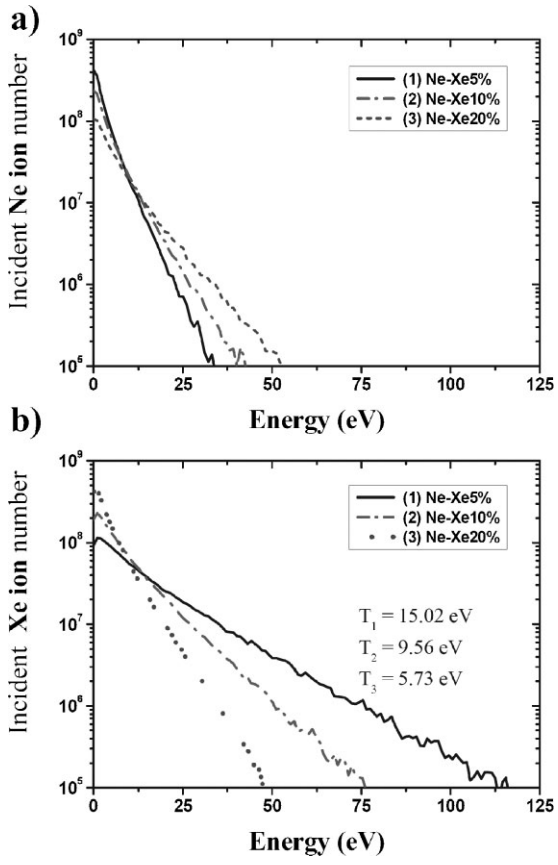

Figure 10. IEDFs (a) of Ne^+ and (b) of Xe^+ impinging on the dielectric surface according to the concentration of Ne/Xe in DBD discharges at 300 Torr.

gaining understanding of the physics of discharges, more efficient and challenging tasks can be conducted in many potential application fields.

Acknowledgements: The authors are grateful to Dr. *P. K. Tiwari* for his comments. This work was supported by the *Korea Science and Engineering Foundation* (*KOSEF*) grant funded by the Korea government (MOST) (No. R01-2007-000-10730-0) and the *Korea Ministry of Education* through its Brain Korea 21 program.

Received: February 5, 2008; Revised: April 29, 2008; Accepted: May 16, 2008; DOI: 10.1002/ppap.200800024

Keywords: atmospheric pressure glow discharges (APGD); energy distribution function; microdischarges; modeling; simulations

[1] M. A. Lieberman, A. J. Lichtenberg, "*Principles of Plasma Discharges and Materials Processing*", 2nd edition, Wiley, New York 2005.
[2] E. Stoffels, I. E. Kieft, R. E. J. Sladek, L. J. M. van den Bedem, E. P. van der Laan, M. Steinbuch, *Plasma Sources Sci. Technol.* **2006**, *15*, S169.
[3] E. Stoffels, A. J. Flikweert, W. W. Stoffels, G. M. W. Kroesen, *Plasma Sources Sci. Technol.* **2002**, *4*, 383.
[4] R. E. J. Sladek, E. Stoffels, R. Walraven, P. J. A. Tielbeek, R. Koolhoven, *IEEE Trans. Plasma Sci.* **2004**, *32*, 1540.
[5] I. E. Kieft, J. L. V. Broers, V. Caubet-Hilloutou, D. W. Slaaf, F. C. S. Ramaekers, E. Stoffels, *Bioelectromagnetics* **2004**, *25*, 362.
[6] Y. J. Hong, H. S. Ko, G. Y. Park, J. K. Lee, *Comput. Phys. Commun.* **2007**, *177*, 122.
[7] S. H. Lee, S. M. Choi, J. W. Shon, *Comput. Phys. Commun.* **2007**, *177*, 133.
[8] S. S. Yang, S. M. Lee, F. Iza, J. K. Lee, *J. Phys. D: Appl. Phys.* **2006**, *39*, 2775.
[9] S. S. Yang, H. C. Kim, S. W. Ko, J. K. Lee, *IEEE Trans. Plasma Sci.* **2003**, *31*, 596.
[10] Z. Donkó, P. Hartmann, K. Kutasi, *Plasma Sources Sci. Technol.* **2006**, *15*, 178.
[11] Y. Sakiyama, D. B. Graves, *J. Phys. D: Appl. Phys.* **2006**, *39*, 3644.
[12] Y. Sakiyama, D. B. Graves, *J. Appl. Phys.* **2007**, *101*, 073306.
[13] Y. Sakiyama, D. B. Graves, *IEEE Trans. Plasma Sci.* **2007**, *35*, 1279.
[14] J. K. Lee, O. V. Manuilenko, N. Yu., Babaeva, H. C. Kim, J. W. Shon, *Plasma Sources Sci. Technol.* **2005**, *14*, 89.
[15] R. Veerasingam, R. B. Campbell, R. T. McGrath, *Plasma Sources Sci. Technol.* **1997**, *6*, 157.
[16] S. Rauf, M. J. Kushner, *J. Appl. Phys.* **1999**, *85*, 3460.
[17] H. C. Kim, F. Iza, S. S. Yang, M. Radmilovic-Radjenovic, J. K. Lee, *J. Phys. D: Appl. Phys.* **2005**, *38*, R283.
[18] C. K. Birdsall, A. B. Langdon, "*Plasma Physics via Computer Simulation*", McGraw-Hill, New York 1985.
[19] J. P. Verboncoeur, *Plasma Phys. Controlled Fusion* **2005**, *47*, A231.
[20] F. Iza, J. K. Lee, M. G. Kong, *Phys. Rev. Lett.* **2007**, *99*, 075004.
[21] J. Choi, F. Iza, J. K. Lee, C. M. Ryu, *IEEE Trans. Plasma Sci.* **2007**, *35*, 1274.
[22] M. Radmilovic-Radjenovic, J. K. Lee, F. Iza, G. Y. Park, *J. Phys. D: Appl. Phys.* **2005**, *38*, 950.
[23] S. M. Lee, S. S. Yang, Y. S. Seo, J. K. Lee, *Plasma Chem. Plasma Process* **2007**, *27*, 349.
[24] F. Iza, G. J. Kim, S. M. Lee, J. K. Lee, J. L. Walsh, Y. T. Zhang, M. G. Kong, *Plasma Process. Polym.* **2008**, *5*, 322.

© 2008 WILEY-VCH Verlag GmbH & Co. KGaA, Weinheim